Isothermal flame balls

Éva Jakab,[1] Dezső Horváth,[1] John H. Merkin,[2] Stephen K. Scott,[3] Péter L. Simon,[3] and Ágota Tóth[1]
[1]*Department of Physical Chemistry, University of Szeged, P.O. Box 105, Szeged H-6701, Hungary*
[2]*Department of Applied Mathematics, University of Leeds, Leeds LS2 9JT, United Kingdom*
[3]*Department of Chemistry, University of Leeds, Leeds LS2 9JT, United Kingdom*
(Received 1 March 2002; published 15 July 2002)

The existence of steady, spherically symmetric wave fronts (''isothermal flame balls'') in chemical reaction systems exhibiting autocatalysis is demonstrated. Such solutions require relatively high kinetic orders p with respect to the autocatalytic species, with $p>5$, but occur even with equal diffusion coefficients. The flame balls are unstable, but have relevance as they indicate the minimum size for a perturbation to initiate a propagating front. A flame ball radius R_b is identified and the dependence of this quantity on the autocatalytic order is determined. This shows R_b tending to infinity as $p\to 5^+$ and as $p\to\infty$, with a minimum for $p\approx 6.71$. Numerical computations are confirmed by asymptotic analysis appropriate for $p\to 5^+$ and for systems with p large.

DOI: 10.1103/PhysRevE.66.016207 PACS number(s): 89.75.Kd, 47.54.+r, 02.30.Mv, 82.33.Vx

I. INTRODUCTION

The propagation of constant-velocity, constant-form traveling waves in chemical systems driven by autocatalytic kinetics has been of considerable interest since the work of Fisher and Kolmogorov [1–5]. In part, this interest derives from the importance of such reaction-diffusion solutions in biological situations such as nerve signal transmission or muscle contraction (see [6–10], for example). Chemical autocatalysis can be represented by a model ''mass action'' process converting a reactant A to an autocatalytic product B according to the stoichiometry

$$A+pB\to(p+1)B \tag{1}$$

with a rate r given by $r=kab^p$, where k is a rate coefficient, a and b are the concentrations of reactants A and B, and p is the order of the reaction with respect to the autocatalytic species [11].

The nature of the traveling wave solution, its selection, and its development from localized initial inputs of autocatalysts for such systems has been studied in some detail by Merkin, Needham, and co-workers in a series of papers [12–17]. For the case of so-called *cubic* autocatalysis (with $p=2$) with equal species diffusion coefficients, an interesting observation [15] for reaction domains with spherical geometry is that there exists some critical radius R_{cr} such that if the localized input extends over a region of radius $R>R_{cr}$, a traveling wave solution is eventually established, but if $R<R_{cr}$ then no traveling wave solution develops and the system returns to its original state. This result was extended in [17] in which it was shown that, if $p>1+2/N$ (where N is the space dimension), then a threshold on the autocatalyst input was needed before waves could form. These results imply the existence of a separatrix between the two types of large time development.

Such a solution of similar equations has been noted previously in a different context: Zel'dovich [18] showed that the classic reaction-diffusion-conduction equations for a premixed laminar flame also have a steady-state solution in spherical geometry. These solutions, known as ''flame balls'' in the combustion context, have been investigated theoretically [19,20] and have been shown to be unstable in the adiabatic case. Even so, such steady-state structures could have relevance in terms of determining the growth or decay of flames from specific initial conditions. We may also note that volumetric heat loss may cause a stabilization of the flame ball structures [21] and that stable flame balls appear to have been recently observed experimentally under microgravity conditions [22–24]. For terrestrial conditions, flame ball solutions cannot be maintained in combustion systems due to the inevitable influence of natural convective effects arising from the production of hot gaseous products.

The analogy between thermal feedback in exothermic combustion and chemical feedback in isothermal autocatalytic systems has been noted previously [25–27]. In this paper, therefore, we investigate the existence of isothermal flame balls in the model autocatalytic scheme (1). Such chemical reactions can be studied experimentally in gels to suppress convection under normal laboratory conditions. In the absence of subsequent reaction steps involving the autocatalyst, the chemical system is analogous to an adiabatic combustion system. This simple model is investigated to determine the conditions under which steady, radially symmetric solutions can exist. The equations governing these steady solutions can be combined to give a simple relation connecting the concentrations of A and B. This relation can then be used to reduce the problem to the consideration of a single equation for the concentration of B. A further scaling of this equation shows that it can be expressed in a universal form, independent of the ratio of the diffusion coefficients of A and B. This is not the case for the corresponding initial-value problem. A necessary condition for the existence of a solution with the appropriate ''smoothness'' at large distances is $p>5$. For $1\leqslant p<5$, there are steady solutions which have compact support with a discontinuity in the derivative at a finite distance.

II. EQUATIONS

The equations governing the reaction and diffusion of the two reactants A and B are (see [3,5,11], for example)

$$\frac{\partial a}{\partial t}=D_A\nabla^2 a-kab^p, \quad \frac{\partial b}{\partial t}=D_B\nabla^2 b+kab^p, \tag{2}$$

where D_A and D_B are the diffusion coefficients of A and B respectively, subject to the condition that

$$a\to a_0, \quad b\to 0 \quad \text{as} \quad |\mathbf{x}|\to\infty \tag{3}$$

together with boundedness conditions at the origin and that

$$a=a_0, \quad b=0 \quad \text{at} \quad t=0 \tag{4}$$

except in some local region, centered on the origin, where there is some input of B to start a reaction. We make Eqs. (2) dimensionless using the reaction time $(ka_0^p)^{-1}$ and a length scale based on this and D_A, namely, we put

$$a=a_0\bar{a}, \quad b=a_0\bar{b}, \quad \bar{t}=(ka_0^p)t, \quad \bar{\mathbf{x}}=\mathbf{x}\left(\frac{ka_0^p}{D_A}\right)^{1/2}. \tag{5}$$

This leads to the dimensionless equations (on dropping the bars for convenience)

$$\frac{\partial a}{\partial t}=\nabla^2 a-ab^p, \quad \frac{\partial b}{\partial t}=D\nabla^2 b+ab^p, \tag{6}$$

where $D=D_B/D_A$. We also impose the condition $p\geqslant 1$ to ensure that the reaction terms are Lipschitz continuous.

We are concerned here with steady solutions to Eqs. (6), i.e., with solutions to the equations

$$\nabla^2 a-ab^p=0, \quad D\nabla^2 b+ab^p=0 \tag{7}$$

subject to

$$a,b \ \text{ continuous at } \ |\mathbf{x}|=0, \quad a\to 1, \ b\to 0 \ \text{ as } \ |\mathbf{x}|\to\infty. \tag{8}$$

We can add Eqs. (7) to eliminate the reaction terms, obtaining $\mathrm{div}(\nabla a+D\nabla b)=0$. The resulting equation can be integrated twice to get, assuming uniform conditions at large distances (i.e., $\nabla a,\nabla b\to 0$ as $|\mathbf{x}|\to\infty$) and applying Eq. (8),

$$a+Db=1. \tag{9}$$

This result can also be deduced from the uniqueness for solutions of Laplace's equation, since $w=a+Db$ satisfies $\nabla^2 w=0, w\to 1$ as $|\mathbf{x}|\to\infty$ and has the (unique) solution $w\equiv 1$. We can then use expression (9) to eliminate a from Eq. (7) and obtain a single equation for b, namely,

$$D\nabla^2 b+(1-Db)b^p=0. \tag{10}$$

We now apply the further scaling

$$u=Db, \quad \tilde{\mathbf{x}}=D^{-p/2}\mathbf{x}. \tag{11}$$

This results in the equation

$$\nabla^2 u+(1-u)u^p=0 \tag{12}$$

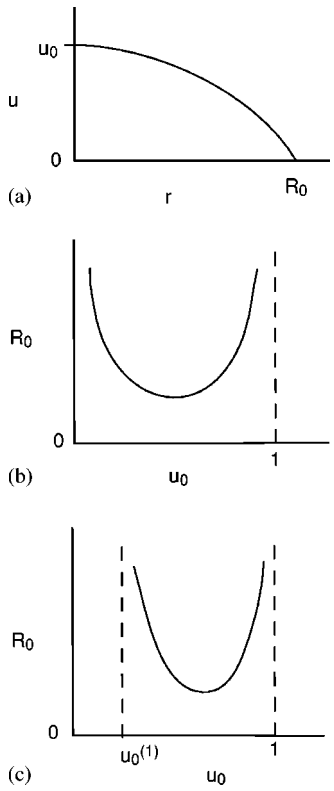

FIG. 1. (a) A schematic representation of the form that the solutions take for $1\leqslant p<5$ or $p>5$, $u_0>u_0^{(1)}$ showing where the solution first becomes zero at R_0. Plots of R_0 against u_0 for (b) $1\leqslant p<5$, (c) $p>5$.

(differentiation with respect to $\tilde{\mathbf{x}}$). It is the nature of the solutions to Eq. (12) that we now consider.

III. STEADY SOLUTIONS

We note that $u\equiv 0$ is a steady solution and that all positive steady solutions are radially symmetric [28], i.e., they satisfy on $\mathcal{R}^N$,

$$u''+\frac{(N-1)}{r}u'+(1-u)u^p=0, \quad u'(0)=0,$$

$$u\to 0 \ \text{ as } \ r\to\infty, \tag{13}$$

and have $u'(r)<0$ on $0<r<\infty$, where r measures the distance from the origin and where primes denote differentiation with respect to r.

It is the positive, spherically symmetric ($N=3$) solutions to Eq. (13) that we are concerned with here. These solutions have been characterized by [29] through the value $R_0(u_0)$ of r at which the solution first becomes zero, where u_0 is the value of u at $r=0$. The situation is illustrated schematically in Fig. 1. The main point to note from this figure is that for $1\leqslant p<5$ there are no values of u_0 for which there is a solution on $0\leqslant r<\infty$. In this case any solution $\bar{u}(r;R_0)$ of Eq.

(13) becomes zero at a finite value R_0 of r with $\overline{u}(r;R_0)<0$ for $r>R_0$. This is not the case for $p>5$. Now there is a range of values for u_0, $0<u_0<u_0^{(1)}<1$, which give solutions $u(r)$ that are nonzero on $0\leqslant r<\infty$ and satisfy the required boundary conditions as $r\to\infty$. Note that $u_0^{(1)}\to 0$ as $p\to 5^+$ and increases with p.

The solutions $u(r)$ of Eq. (13) for $0<u_0\leqslant u_0^{(1)}, p>5$ can be one of the two general types identified in [30]. These can be *slow decaying solutions*, which, in the present case, have

$$u\sim r^{-2/(p-1)} \quad \text{as} \quad r\to\infty$$

or *ground states* (*fast decaying solutions*), which have

$$u\sim r^{-1} \quad \text{as} \quad r\to\infty.$$

For a given value of p (>5) the ground state solution is unique, i.e., there is only one value of u_0 in $0<u_0\leqslant u_0^{(1)}$ which gives rise to a ground state solution.

Before we consider our numerical investigation of Eq. (13) we mention the results concerning the traveling waves that can arise as long time behavior of initial-value problem (6). For $D=1$ the two time-dependent equations can be combined into a single equation for b (say) using Eq. (9). This is not the case for $D\neq 1$, where no such simplification is possible and the full two-variable system has to be considered [31]. It was shown in [15] for the spherically symmetric case with $D=1$ that traveling waves are initiated for any input $u_0 g(r)>0$ for $1\leqslant p<5/3$ [where the function $g(r)$ is nonzero only on some finite range of r and has a maximum value of unity]. However, for $p>5/3$ a threshold input was required, i.e, $u_0>u_0^{min}$ was needed. The nature of the resulting traveling waves was discussed in [17], where it was shown that the wave speed c decreased monotonically with increasing p and that the solution became singular as $p\to 1$, with $c\sim 2+O([p-1]^{2/3})$ for $(p-1)$ small. We can extend the radially symmetric solutions $\overline{u}(r;R_0)$ beyond R_0 by taking $\overline{u}(r;R_0)=0$ for $r>R_0$. These solutions are then subsolutions for the initial-value problem (6). Fife [32] has shown that, if $u(\mathbf{x},0)\geqslant\overline{u}(r;R_0)$, then $u(\mathbf{x},t)\to 1$ as $t\to\infty$ uniformly in compact sets in $\mathcal{R}^N$, thus giving a sufficient condition for the initiation of traveling waves.

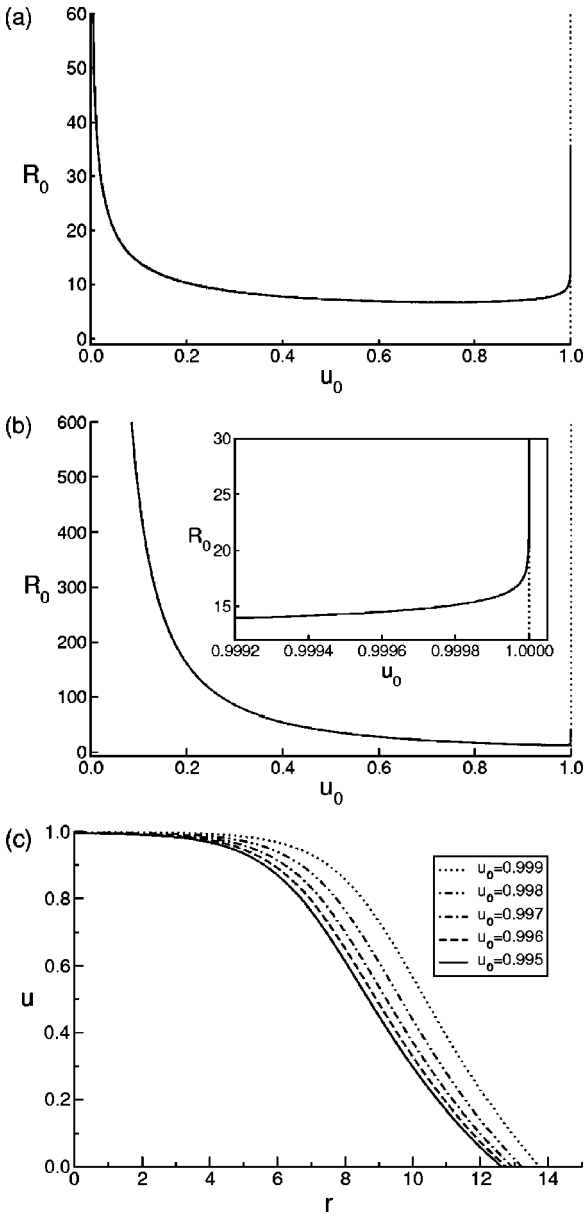

FIG. 2. R_0, the value where the solution is zero, plotted against u_0 for (a) $p=2$, (b) $p=4$. (c) Solutions $\overline{u}(r;R_0)$ for values of u_0 slightly less than unity for $p=4$.

A. Numerical simulations

We start by calculating $R_0(u_0)$, the results are shown in Figs. 2 and 3. Figure 2(a) (for $p=2$) shows that R_0 increases as $u_0\to 0$, changes only relatively slowly for $0.2<u_0<0.95$, and rises very steeply as $u_0\to 1$ from below. For $p=4$ [Fig. 2(b)] the values of R_0 are somewhat larger than those for $p=2$ and the rapid increase in R_0 as $u_0\to 1$ is even more pronounced. The behavior close to $u_0=1$ is expanded in the inset in Fig. 2(b). Solutions $\overline{u}(r;R_0)$ for u_0 close to unity are displayed in Fig. 2(c), showing how R_0 increases as $u_0\to 1$.

In Fig. 3 we plot R_0 against u_0 for $p=5$, 6, and 7. There is again a very sharp rise in R_0 close to $u_0=1$ (not really seen in the figure), though now for $p=6$, 7 the curves have vertical asymptotes at values of $u_0>0$ (at $u_0\simeq 0.75$ for $p=6$ and at $u_0\simeq 0.92$ for $p=7$). For $p=5$ the curve still approaches the R_0 axis as $u_0\to 0$ though with much greater values of R_0 than for the two previous cases.

We next consider numerical solutions to Eq. (13), looking for *ground state* solutions. The form that these solutions take for large and small r can be found by substituting the appropriate expansions into Eq. (13) and equating like powers of r. We find that

$$u(r)\sim\frac{A_0}{r}-\frac{A_0^p}{(p-2)(p-3)r^{p-2}}+\cdots \quad \text{as} \quad r\to\infty \quad (p>5) \tag{14}$$

for some positive constant A_0, and have, since $u'(0)=0$,

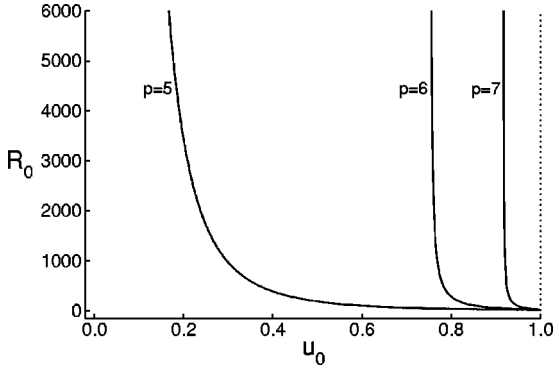

FIG. 3. R_0, the value where the solution is zero, plotted against u_0 for $p=5$, 6, 7.

$$u(r)=u_0-\frac{(1-u_0)u_0^p}{6}r^2 - \frac{u_0^{2p-1}(1-u_0)[u_0-p(1-u_0)]}{120}r^4+\cdots \quad (15)$$

as $r\to 0$.

Expression (15) shows that we must have $u_0<1$. If $u_0=1$, then we get the trivial solution $u(r)\equiv 1$, which does not satisfy the outer boundary conditions. If $u_0>1$, then $u(r)$ must increase with r for r small. To satisfy the outer boundary conditions $u(r)$ must have a local maximum at $r=r_1$ (say), where $r_1>0$ and $u(r_1)>1$, $u'(r_1)=0$,$u''(r_1)\leqslant 0$. However, from Eq. (13) $u''(r_1)=[u(r_1)-1]u(r_1)^p>0$, giving a contradiction. A consequence of this result is that $0\leqslant u(r)<1$ on $0<r<\infty$.

The solutions for large and small r given by Eqs. (14) and (15) were joined numerically using a standard shooting method for solving boundary-value problems. The solution was calculated at $r=0.001$ using Eq. (15) and this was extended numerically using the CVODE package [33]. The value of u_0 was adjusted until the behavior given by Eq. (14) was approached at a large value of r. We found that taking $r=200.0$ gave sufficient accuracy. This procedure determines the values of u_0 and A_0 for a given value of p. Typical profiles are shown in Fig. 4. The figure shows that the profiles become more spread out for larger values of p, with u_0 also increasing with p. This latter point is brought out more clearly in Fig. 5, where we plot u_0 against p. The graph shows that $u_0\to 1$ for $p\gg 1$ and suggests that u_0 approaches zero as $p\to 5$ from above. The values obtained for u_0 of $u_0=0.7533$ for $p=6$ and $u_0=0.9166$ for $p=7$ correspond to the vertical asymptotes in Fig. 3. This suggests that the maximum values of u_0 for which a solution on $0<r<\infty$ is possible give the ground states. For values of u_0 less than this maximum we obtain the slow decaying solutions, which have $u\sim r^{-2/(p-1)}$ for r large.

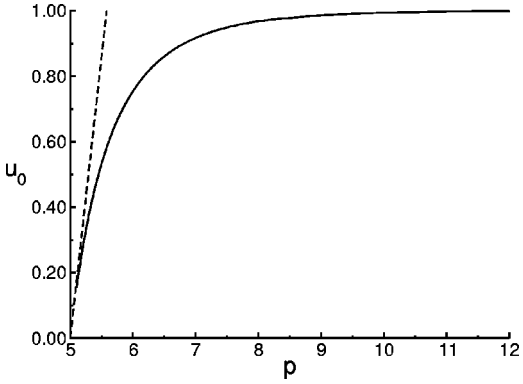

FIG. 5. A graph of u_0 against p obtained from the numerical integration of Eq. (13) (full line). Asymptotic expression (42) for $(p-5)$ small is shown by the broken line.

We now consider these two limiting forms, starting by looking at the nature of the solution for p large.

B. Solution for p large

The structure of the solution for p large is illustrated in Fig. 6, where we plot $u(r)$ for $p=40.0$. This figure shows that, with $p\gg 1$, there is an inner region where $u(r)\equiv 1$ and a ''reaction region'' centred on $r=X(p)$, with $X(p)\gg 1$ for $p\gg 1$. This suggests that we make the transformation

$$r=X(p)+\overline{r}, \quad X=p\overline{X}, \quad \text{with} \quad \overline{X} \text{ of } O(1) \text{ for } p\gg 1. \quad (16)$$

The reason for the scaling for X will become apparent below.

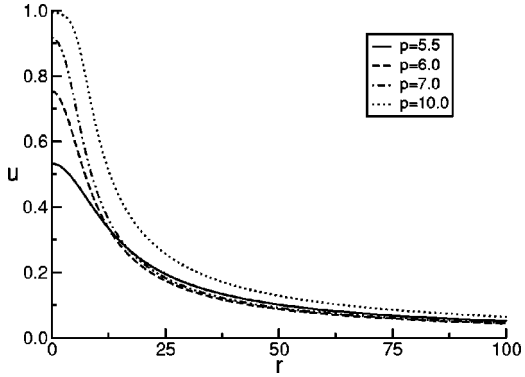

FIG. 4. Solutions $u(r)$, satisfying Eqs. (14) and (15), obtained from the numerical integration of Eq. (13) for $p=5.5$, $p=6$, $p=7$ and $p=10$.

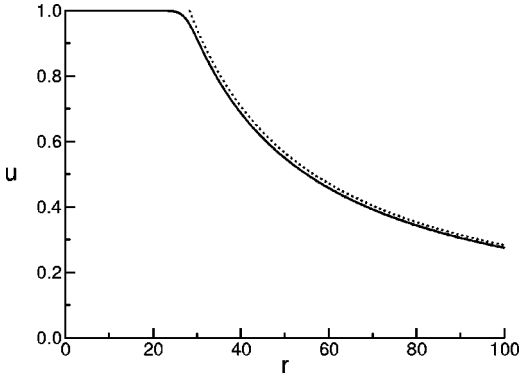

FIG. 6. A graph of $u(r)$ for $p=40$ to illustrate the structure of the solution for p large, obtained from the numerical integration of Eq. (13).

When transformation (16) is substituted into Eqs. (13), we find that the resulting equations have a two-layer structure. There is an inner layer where $\bar{r}$ is left unscaled and in which we put $u=1-B/p$. We then look for a solution by expanding B and $\bar{X}$ in inverse powers of p. The leading-order terms $(B_0,\bar{X}_0)$ are all that we really need to consider. These satisfy, on letting $p\to\infty$,

$$B_0''-B_0\mathrm{e}^{-B_0}=0, \quad B_0\to 0 \ \text{ as } \ \bar{r}\to-\infty. \tag{17}$$

Primes now denote differentiation with respect to $\bar{r}$. From Eq. (17) it follows that

$$B_0'^2=2[1-(1+B_0)\mathrm{e}^{-B_0}] \tag{18}$$

and then

$$B_0\sim\sqrt{2\bar{r}}+\cdots, \quad \text{hence } \ u\sim 1-\frac{\sqrt{2\bar{r}}}{p}\cdots \quad \text{as } \ \bar{r}\to\infty. \tag{19}$$

The expression for u in Eq. (19) suggests the scaling $\zeta=\bar{r}/p$ for the outer layer, with u left unscaled in this region. In this outer layer $u<1$ and hence $u^p\to 0$ as $p\to\infty$. Then, to get a viable solution in the outer region both terms arising from the diffusion must balance. This, together with the scaling of $\bar{r}$ for the outer region, requires that X be of $O(p)$. The equation at leading order for this region is

$$u''+\frac{2}{\bar{X}_0+\zeta}u'=0, \tag{20}$$

subject to, from Eqs. (13) and (19),

$$u\sim 1-\sqrt{2}\zeta+\cdots \quad \text{as } \ \zeta\to 0, \quad u\to 0 \quad \text{as } \ \zeta\to\infty \tag{21}$$

(primes denote differentiation with respect to ζ). The required solution is

$$u=\frac{\bar{X}_0}{(\bar{X}_0+\zeta)}. \tag{22}$$

Matching Eq. (22) with the inner layer Eq. (21) then gives

$$\bar{X}_0=\frac{1}{\sqrt{2}}, \quad \text{hence} \quad X\sim\frac{p}{\sqrt{2}}+O(1) \quad \text{for } \ p\gg 1. \tag{23}$$

C. Solution as $p\to 5$

To obtain a solution to Eq. (13) valid as $p\to 5$ from above, we put

$$p=5+\delta, \quad 0<\delta\ll 1. \tag{24}$$

The numerical integrations indicate that both u_0 and $u(r)$ decrease in size as $p\to 5$ (see Fig. 5). This, together with Eq. (13), suggests that we introduce the scaling

$$u=\delta^m U, \quad y=\delta^{2m}r, \tag{25}$$

where the exponent m $(m>0)$ is to be determined. Applying Eq. (25) in Eq. (13) gives

$$U''+\frac{2}{y}U'+(1-\delta^m U)U^5\exp[\,\delta(\ln U+m\ln\delta)]=0. \tag{26}$$

Now primes denote differentiation with respect to y.

First suppose that $m<1$. Equation (26) then suggests looking for a solution by expanding

$$U(y;\delta)=U_0(y)+\delta^m U_1(y)+O(\delta,\delta\ln\delta). \tag{27}$$

At leading order we obtain

$$U_0''+\frac{2}{y}U_0'+U_0^5=0. \tag{28}$$

For y small

$$U_0=b_0-\frac{b_0^5 y^2}{6}+\cdots \tag{29}$$

for some constant b_0 to be determined. We can scale b_0 out of the leading-order problem (28), (29) by putting

$$U_0=b_0\bar{U}_0, \quad \bar{y}=b_0^2 y. \tag{30}$$

$\bar{U}_0$ satisfies Eq. (28) (with y replaced by $\bar{y}$) and has

$$\bar{U}_0=1-\frac{\bar{y}^2}{6}+\frac{\bar{y}^4}{24}+\cdots, \quad \bar{y} \text{ small},$$

$$\bar{U}_0\sim\frac{C_0}{\bar{y}}-\frac{C_0^5}{6\bar{y}^3}+\cdots, \quad \bar{y} \text{ large}. \tag{31}$$

A solution to Eq. (28), satisfying Eq. (31), can be determined numerically as an initial-value problem starting with $\bar{y}$ small. This gives $C_0=1.7321$.

At $O(\delta^m)$ we obtain

$$U_1''+\frac{2}{y}U_1'+5U_0^4U_1=U_0^6. \tag{32}$$

Equation (32) has a complementary function

$$\tilde{U}=2yU_0'+U_0, \tag{33}$$

which satisfies the required boundary conditions [$\tilde{U}$ bounded at $y=0$ and has $\tilde{U}$ of $O(y^{-1})$ for y large]. Thus, if we write Eq. (32) in the self-adjoint form $(d/dy)(y^2U_1')+5y^2U_0^4U_1=y^2U_0^6$, we can see that it has a solution only if the compatibility condition

$$\int_0^\infty U_0^6\tilde{U}y^2dy=\int_0^\infty(2y^3U_0^6U_0'+y^2U_0^7)dy=0 \tag{34}$$

is satisfied. If we integrate by parts the term involving U_0', we find that this condition is *not* satisfied, the integral becomes $\frac{1}{7}\int_0^\infty y^2 U_0^7 dy > 0$.

Thus we must take $m=1$, with scaling (25) becoming

$$u=\delta U, \quad y=\delta^2 r. \tag{35}$$

An expansion of the form

$$U(y;\delta)=U_0(y)+\delta(\ln \delta U_1(y)+U_2(y))+\cdots \tag{36}$$

is now suggested. At leading order we again get Eq. (28), rescaled by Eq. (30) to remove the constant b_0. At $O(\delta \ln \delta)$ we obtain

$$U_1''+\frac{2}{y}U_1'+5U_0^4U_1=-U_0^5. \tag{37}$$

The compatibility condition equivalent to Eq. (34) is now that

$$\int_0^\infty U_0^5 \tilde{U} y^2 dy=\int_0^\infty (2y^3U_0^5U_0'+y^2U_0^6)dy=0. \tag{38}$$

Now integrating by parts the term involving U_0' shows that this condition *is* satisfied and a solution at this order is possible.

At $O(\delta)$ we obtain

$$U_2''+\frac{2}{y}U_2'+5U_0^4U_2=U_0^5(U_0-\ln U_0). \tag{39}$$

We rescale Eq. (39) using Eq. (30) and $U_2=b_0\overline{U}_2$ to obtain

$$\overline{U}_2''+\frac{2}{y}\overline{U}_2'+5\overline{U}_0^4\overline{U}_2=\overline{U}_0^5(b_0\overline{U}_0-\ln \overline{U}_0-\ln b_0). \tag{40}$$

The compatibility condition now becomes

$$\int_0^\infty \overline{U}_0^5(b_0\overline{U}_0-\ln \overline{U}_0-\ln b_0)\tilde{U}\overline{y}^2 d\overline{y}$$
$$=\frac{b_0}{7}\int_0^\infty \overline{y}^2\overline{U}_0^7 d\overline{y}-\frac{1}{6}\int_0^\infty \overline{y}^2\overline{U}_0^6 d\overline{y}=0. \tag{41}$$

It is this condition that determines the value of b_0. Numerical integration gives $b_0=1.7181$.

The solution at $O(\delta)$ is not unique, any multiple of $\tilde{U}$ can be added. We expect the arbitrariness at this order to be resolved at higher terms in the expansion (36).

The above analysis shows that the solution has a weak logarithmic singularity as $p\to 5^+$ with

$$u_0 \sim 1.7181\delta+O(\delta^2, \delta^2 \ln \delta) \tag{42}$$

as $\delta=(p-5)\to 0$. A graph of asymptotic expression (42) is plotted in Fig. 5 (the broken line), showing agreement with the numerically determined values as p decreases towards 5.

We can use this approach to explain why $p=5$ is the critical exponent for $N=3$. Consider a general value p_0 for p $(p_0>1)$ and put $p=p_0+\delta$ $(0<\delta\ll 1)$. The above analysis suggests that we first make the transformation

$$u=\delta U, \quad y=\delta^{(p_0-1)/2} r \tag{43}$$

and expand as in Eq. (36). The corresponding leading-order equation is, for a general geometric dimension N,

$$U_0''+\frac{(N-1)}{y}U_0'+U_0^{p_0}=0 \tag{44}$$

[satisfying conditions equivalent to Eq. (31), the modification to transformation (30) is $\overline{y}=b_0^{(p_0-1)/2}y$].

It is the term at $O(\delta \ln \delta)$ that is the important one to consider. We note that a term of this order will always appear in any asymptotic expansion for small δ as it arises from the scaling of u in Eq. (43) in which δ is raised to the power δ. The corresponding equation is

$$U_1''+\frac{(N-1)}{y}U_1'+p_0U_0^{p_0-1}U_1=-U_0^{p_0}. \tag{45}$$

Equation (45) has a complementary function

$$\tilde{U}=\left(\frac{p_0-1}{2}\right)yU_0'+U_0 \tag{46}$$

equivalent to Eq. (33), which satisfies the required boundary conditions. This then leads to the compatibility condition that

$$\int_0^\infty U_0^{p_0}\tilde{U}y^{N-1}dy=\frac{p_0(2-N)+(N+2)}{2(p_0+1)}$$
$$\times\int_0^\infty y^{N-1}U_0^{p_0+1}dy=0, \tag{47}$$

provided $N>2$. This gives the critical exponent

$$p_0=\frac{N+2}{N-2} \quad (N>2). \tag{48}$$

Expression (48) gives $p_0=5$ when $N=3$ and suggests that the isothermal flame balls are a direct consequence of having spherical geometry and will not arise in either planar or cylindrical geometries.

IV. STRUCTURE OF THE SOLUTION

The above analysis confirms the existence of steady isothermal flame ball solutions for the reaction-diffusion system driven by an autocatalytic reaction of sufficiently high order ($p>5$). Although such autocatalytic orders are not common in simple solution-phase chemical systems, values for p in the relevant range have been reported for a model representation of systems with micellar and phase-transfer autocatalysis [34–37]. The results given here also extend in a formal manner the results presented previously by Merkin and Needham for lower autocatalytic powers, and also provide a connection to the behavior of nonisothermal systems driven by the Arrhenius temperature dependence of reaction rate coefficients.

The steady-state profiles identified here are unstable solutions of the corresponding initial-value problem. As such, they are still of distinct practical interest as they identify the critical ''watershed'' between initial conditions for which propagating reaction fronts can develop and those for which initiation fails. It is thus of interest to determine how the ''size'' of the steady state flame ball varies with the autocatalytic power p. To make this question precise, we define a reaction rate per unit radial distance, $v_r=r^2u^p(1-u)$. For $D_A=D_B$, this is equivalent to the function r^2ab^p. This function is plotted as a function of the radial distance r for several values of the autocatalytic order p in Fig. 7(a). We then define the ''radius'' of the flame ball in terms of the location R_b at which this function has a maximum for any given value of p. The resulting variation of R_b with p is shown in Fig. 7(b). This shows a rapid decrease in radius as p increases from $p=5$, with a minimum radius at $p\simeq 6.71$. For higher autocatalytic orders, the radius increases, showing an approach to a constant slope of ≈ 0.7 for p large. This linear growth at high p is consistent with the asymptotic analysis which predicts a slope of $1/\sqrt{2}$ [expression (23)].

The analysis of the preceding section provides insights into how the steady solution changes as p increases from $p=5$. For values of p just above $p=5$ the autocatalyst concentration takes only small values throughout, of $O(p-5)$ from Eq. (35). However, the profiles extend over large distances from the center, of $O([p-5]^{-2})$. As p increases the autocatalyst concentration increases, approaching a constant value at the center, with the extent of the profile decreasing. For even larger values of p, a fully reacted core region develops and the outer structure is purely diffusive. There is a relatively thin reaction zone between these two regions. This behavior is apparent in Fig. 7(a) for the higher values of p, which reveals the development of the central core and also shows that the maximum value of v_r increases with p.

In Fig. 7(c), we plot the location R_V of the maximum of the volumetric reaction rate $V=u^p(1-u)$. For low autocatalytic powers ($p\simeq 5$), this maximum occurs at the center of the sphere, $R_V=0$, but as p increases, the maximum moves away from the center at $p=6.55$, indicating the initial onset of the central core region. This onset is apparently linked to the minimum in R_b.

The origin of the growth as $p\to 5^+$ can be understood from Eq. (13). If we multiply this Eq. (with $N=3$) by r^2, integrate and apply conditions (14) and (15), we obtain

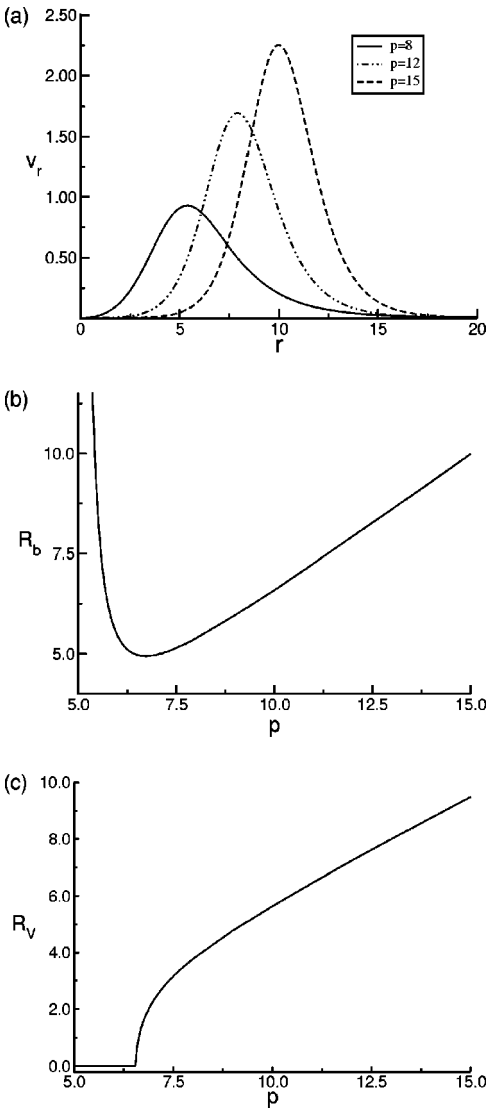

FIG. 7. (a) A graph of v_r, the reaction rate per unit radial distance, for a range of values of p. (b) R_b, the position where v_r achieves its maximum value, plotted against p. (c) R_V, the position where the volumetric reaction rate $V=u^p(1-u)$ achieves its maximum value, plotted against p.

$$A_0=\int_0^\infty r^2u^p(1-u)dr \tag{49}$$

with the value of A_0 providing an estimate for R_b. From Eqs. (30), (31), and (35)

$$A_0\sim\frac{C_0}{b_0\delta}+\cdots=1.008\delta^{-1}+\cdots \quad \text{as} \quad \delta\to 0 \tag{50}$$

(where $\delta=p-5$).

Equation (13), which we considered in detail, was derived from the original dimensional version by a nonstandard transformation. The autocatalyst concentration is made dimensionless with a weighting of diffusion coefficients, $b=u(D_A/D_B)a_0$. A similar sort of weighting is used for the dimensionless spatial variable

$r=(ka_0^p/D_B)^{1/2}(D_A/D_B)^{p/2}x$. Thus larger autocatalyst concentrations will be achieved when the value of D_A is greater relative to that of D_B. This is to be expected as, in this case, the substrate can diffuse more easily into the reaction region, thus producing more autocatalyst. The radial spread of the profiles is also affected by the ratio of the diffusion coefficients, being generally greater in extent, the larger the value of D_A is relative to D_B. This effect becomes more pronounced for the higher order autocatalysis.

ACKNOWLEDGMENTS

This work was supported by the British Council and the Hungarian Scholarship Board (Ministry of Education) under their Joint Academic Research Programme and by the ESF Scientific programme REACTOR. A.T. and D.H. thank the Ministry of Education (FKFP 0004/2001) and the Hungarian Scientific Research Fund (OTKA F031728) for financial support.

[1] R.A. Fisher, Ann. Eugenics **7**, 355 (1937).
[2] A.N. Kolmogorov, I.G. Petrovskii, and N.S. Piskunov, Bjull. Moskovskovo, Gos. Univ. **17**, 1 (1937).
[3] S.K. Scott, *Chemical Chaos* (Clarendon Press, Oxford, 1991).
[4] R. Kapral and K. Showalter, *Chemical Waves and Patterns* (Kluwer, Dordrecht, 1995).
[5] K. Showalter, Nonlinear Sci. Today **4**, 3 (1995).
[6] R. Fitzhugh, in *Biological Engineering*, edited by H. P. Schwan (McGraw-Hill, New York, 1969).
[7] N. F. Britton, *Reaction-Diffusion Equations and their Apppllications to Biology* (Academic, London, 1986).
[8] J. D. Murray, *Mathematical Biology* (Springer, Berlin, 1989).
[9] A. Goldbeter, *Biochemical Oscillations and Cellular Rhythms* (Cambridge University Press, Cambridge, 1996).
[10] J. P. Keener and J. Sneyd, *Mathematical Physiology* (Springer, New York, 1998).
[11] P. Gray and S.K. Scott, *Chemical Oscillations and Instabilities: Non-Linear Chemical Kinetics* (Clarendon Press, Oxford, 1990).
[12] J.H. Merkin and D.J. Needham, J. Eng. Math. **23**, 343 (1989).
[13] J.H. Merkin and D.J. Needham, Proc. R. Soc. London, Ser. A **430**, 315 (1990).
[14] P. Gray, J.H. Merkin, D.J. Needham, and S.K. Scott, Proc. R. Soc. London, Ser. A **430**, 509 (1990).
[15] D.J. Needham and J.H. Merkin, Nonlinearity **5**, 413 (1992).
[16] J. Billingham and D.J. Needham, Q. Appl. Math. **50**, 343 (1992).
[17] J.H. Merkin and D.J. Needham, Z. Angew. Math. Phys. **44**, 707 (1993).
[18] Y.B. Zel'dovich, *Theory of Combustion and Detonation of Gases* (Academy of Sciences, Moscow, 1944).
[19] J.D. Buckmaster and S. Weeratunga, Combust. Sci. Technol. **35**, 287 (1984).
[20] B. Deshaies and G. Joulin, Combust. Sci Technol. **37**, 99 (1984).
[21] J.D. Buckmaster, G. Joulin, and P.D. Ronney. Combust. Flame **84**, 411 (1991).
[22] P.D. Ronney, Combust. Flame **82**, 1 (1990).
[23] P.D. Ronney, K.N. Whaling, A. Abbud-Madrid, J.L. Gatto, and V.L. Pisowicz, AIAA J. **32**, 569 (1994).
[24] P.D. Ronney, M-S. Wu, H.G. Pearlman, and K.J. Weiland, AIAA J. **36**, 1361 (1998).
[25] P. Gray and S.K. Scott, Chem. Eng. Sci. **39**, 1087 (1984).
[26] A. D'Anna, P.G. Lignola, and S.K. Scott, Proc. R. Soc. London, Ser. A **404**, 341 (1986).
[27] S.K. Scott and K. Showalter, J. Phys. Chem. **22**, 8702 (1992).
[28] B. Gidas, W. Ni, and L. Nirenberg, Commun. Math. Phys. **68**, 209 (1979).
[29] T. Ouyang and J. Shi, J. Diff. Eqns. **158**, 94 (1999).
[30] L. Erbe and M. Tang, J. Diff. Eqns. **138**, 351 (1997).
[31] J. Billingham and D.J. Needham, Philos. Trans. R. Soc. London, Ser. A **336**, 497 (1991).
[32] P.C. Fife, *Mathematical Aspects of Reacting and Diffusing Systems*, Lecture Notes in Biomathematics Vol. 28 (Springer-Verlag, Berlin, 1979).
[33] S.D. Cohen and A.C. Hindmarsh, Comput. Phys. **10**, 138 (1996).
[34] P.A. Bachmann, P.L. Luisi, and J. Lang, Nature (London) **357**, 57 (1992).
[35] J. Billingham and P.V. Coveney, J. Chem. Soc., Faraday Trans. **90**, 1953 (1994).
[36] T. Buhse, R. Nagarajan, D. Lavabre, and J.C. Micheau, J. Phys. Chem. A **101**, 3910 (1997).
[37] R. Ball and A.D.J. Haymet, Phys. Chem. Chem. Phys. **3**, 4753 (2001).